MASTER'S THESIS

Detection of Partial Discharge in High Voltage Systems using Optical Fibre Bragg Gratings

Ola Byström

Master of Science in Engineering Technology
Media Engineering

Luleå University of Technology
Department of Computer Science, Electrical and Space Engineering

LULEÅ UNIVERSITY OF TECHNOLOGY

Detection of partial discharge in high voltage systems using optical Fibre Bragg Gratings

Ola Byström

Lulea University of Technology
Dept. of Computer Science and Electrical Engineering

8th January 2011

Abstract

For electricity suppliers, a very important goal is to have a stable operation and to consistently and reliably deliver electricity. A big threat to that operation is obviously equipment breakdown that could cause downtime. In high voltage equipment, its insulation could arguably be considered one of the most important component. When electrical insulation deteriorates, small cracks and voids will start to appear within the material. These voids have less insulating ability and will eventually not be able to withstand the high voltage and become conductive and cause equipment breakdown. Before this critical situation occurs, when the deterioration is not enough for the voids and voltage to cause a full arc, there will be small sparks or partial discharges occurring. There are already methods for sensing these partial discharges but this thesis focuses on a new promising method utilizing optical fiber Bragg Gratings as sensors. An advantage with optical sensor being their immunity to electromagnetic interference, making it theoretically possible for them to be placed in harsh environments where conventional methods could not be used.

The project started with researching previously written material on this relatively uncharted area of application and continued on to successfully constructing an optical sensor for ultrasound. The techniques used for that sensor could then be brought into a high voltage lab to conduct testing on generated partial discharges. A new method of mounting the fiber Bragg grating inside an insulation material for testing with partial discharges was created. The results were not final but showed promising potential in this kind of application for optical fiber Bragg gratings to exist.

Preface

This project has been a wonderful and, in many ways, educating personal experience for me. I'd like to thank my supervisors Dr. Le Nguyen Binh and Dr. Tadeusz Czaszejko from Monash University in Melbourne, Australia and Associate Professor Johan Carlson from Lulea University of Technology in Lulea, Sweden for their support throughout my time in Australia while working on this project.

I would also like to thank Mr. Sven Molin, Dr. Le Nguyen Binh and Ms. Pam Dickinson for all their help in making this journey happen.

Ola Byström

Contents

CHAPTER 1

Introduction

1.1 Background and motivation

For electricity suppliers, a reliable delivery of electricity is considered their most important goal. To accomplish this, the stable operation of their equipment is a requirement since failure of major plant items can result in lengthy interruptions and costly repairs [1].

Since the power equipment is operating at very high voltages, its electrical insulation is considered to be a very important material component, which is also what Blackburn et al. writes in their paper [2]. Insulation failure caused by deterioration from mechanical, thermal and electrical stresses is often the reason behind equipment breakdown. Traditionally the detection of such equipment failure has been done by regular maintenance with the equipment taken offline. A system that is able to monitor the equipment while it is online and detect when such a failure is about to happen is therefore desirable. Blackburn et al. suggests that one of the best indicators of insulation failure is the level of partial discharge activity in the insulation material.

Partial discharge usually occurs in the insulation material with the appearance of voids or cracks, or bubbles within liquid insulation, as the insulation ages and deteriorates. A PD is a brief transient electrical breakdown at these imperfections in the insulation material and produces small electrical currents that can be measured and monitored directly electrically. However, due to electromagnetic interference from external sources, these measurements are hard to carry out while the system is online. Using optical fiber as a measuring device, with its immunity to such interference, is therefore an attractive solution. Optical sensors in the form of fiber Bragg gratings have been proven to be effective in measuring material strain, temperature and even sound pressure. It has been shown that partial discharges gives rise to acoustic pulses in the frequency regions of ultrasound [3].

1.2 Goals

The main goal for this thesis was to evaluate and answer the question of the feasibility of using fiber Bragg gratings to measure the acoustic impact from partial discharges and to construct and test a prototype of such a sensor in a high voltage lab. Several other smaller goals were also set such as evaluating different sensing systems, creating a working ultrasound detector, evaluating and testing different materials on where to mount the fiber while sensing partial discharges and investigating the fiber sensor sensitivity. There was always a desire to look at the currently available research and contribute with something new.

1.3 Thesis structure

This report will firstly provide the information needed to understand the rest of the thesis. In chapter two, this background theory will be described for fiber Bragg gratings, optical sensing systems, partial discharge and high voltage systems, ultrasound sensing and wave theory. The following chapter, chapter three, will describe the methods and experiments used in the project including the characterization of the fiber Bragg grating, ultrasound sensing, the confirmation experiment with a laser doppler vibrometer, partial discharge detection and signal processing. The results for these methods will be given in chapter four which consists of topics corresponding with those of chapter three. Finally, in chapter five, conclusions will be drawn and the contributions of the thesis to the related research area will be discussed along with what can be done in the future.

CHAPTER 2

Theory

2.1 Fiber Bragg gratings

A very central component in this project was the fiber Bragg grating (hereby referred to as FBG) which was used as the actual sensor for the ultrasonic sound waves. A paper written by Kenneth O. Hill and Gerald Meltz [4] and another written by Martin Guy [5] describes several methods of producing fiber Bragg gratings. Basically, an FBG is created by exposing a photosensitive fiber core to an intensity pattern of UV light which causes a permanent increase in the core's refractive index, creating a periodic index modulation according to the UV mask pattern. This periodic modulation of the refractive index works as a grating that causes a certain wavelength of incident light to be reflected. The light that is not reflected is transmitted through the grating. An illustration showing this general function of the FBG is shown in fig. 2.1. By reflecting a narrow band of the incident optical field, the FBG will effectively act like an optical bandpass filter (or a bandstop filter depending on which terminal is being observed) with the strongest mode coupling at what is called the Bragg wavelength λ_B given by

$$\lambda_B = 2n_{eff}\Lambda \tag{2.1}$$

where n_{eff} is the effective refractive index, or modal index, and Λ is the grating period. In its most general case, the index perturbation $\delta n(z)$ along the axis of the fiber can be represented by a sinusoidal phase and amplitude modulation given by

$$\delta n(z) = \delta n_0(z)[1 + m\cos(\frac{2\pi z}{\Lambda} + \phi(z))] \tag{2.2}$$

where $\delta n_0(z)$ is the amplitude of the photoinduced index change. Hill and Meltz writes that both the refractive index and the envelope of the grating modulation, and therefore

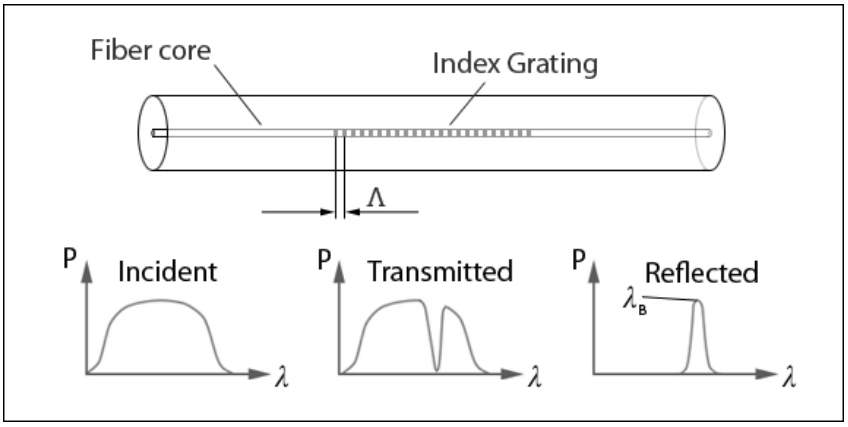

Figure 2.1: Basic FBG function

the modal index n_{eff}, will usually vary along the grating length and that the contrast, determined by the visibility of the UV pattern, is given by the parameter m [4]. The grating can then be represented by adding this index change described in eq. (2.2) to the original refractive index of the core

$$n(z) = n_{core} + \delta n(z). \tag{2.3}$$

Any change in fiber properties that alters the modal index or grating period, such as strain, temperature or polarization, will cause a change the Bragg wavelength λ_B according to eq. (2.1). Strain and temperature will affect the variables in eq. (2.1) based on the elasto-optic and the thermo-optical effects respectively and with these the expression for relative wavelength shift of the bragg wavelength can be expressed as

$$\frac{\Delta\lambda_B}{\lambda_B} = (1 - p_\epsilon)\epsilon_z + (\alpha + \xi)\Delta T \tag{2.4}$$

where p_ϵ is the elasto-optical coefficient, α the coefficient of thermal expansion and ξ the thermo-optical coefficient of the optical fiber. ΔT and ϵ_z are the temperature difference and axial strain of the fiber respectively [6] [7]. These parameters depend on the fiber material and will determine the sensitivity of the grating along with its reflection characteristics in correlation with the sensing system used. Section 3.1 describes a method used to estimate the sensitivity of the grating available for this project.

A few things noted from already published material should be considered before using an FBG as a sensor. It has been shown by Graham Thursby et al. that a FBG sensor generally has a strong directivity, meaning it has the highest sensitivity when the strain waves are acting along the fiber axis [8]. The directivity is not always undesired, as shown in their paper about structure health monitoring using fiber Bragg grating rosettes to estimate the location of a structural damage. In addition to this, it has also been shown, here by Aldo Minardo et al., that for the sensor to stay linear and maintain sensitivity, the

wavelength of the strain wave needs to be much larger than the grating length [9]. This means there is a recommended highest frequency measurable by the sensor depending on its length and in the paper it is recommended to use as short a grating as possible when using it as a sensor for ultrasound.

2.2 Partial discharge and high voltage systems

As mentioned in the introduction, the phenomena that is partial discharge (PD) is an important occurrence in high voltage equipment. Not because it is desired, but because it can be seen as a good indicator of when high voltage electrical insulation is failing.

When electrical insulation ages, it deteriorates from the cumulative effects of mechanical, thermal and electrical stresses. The signs of ageing can be the appearance of voids or cracks, in solid insulation, while bubbles or particles could appear in liquid insulation. When there is voltage across a material it will be subject to a voltage stress field with a strength based on the voltage, the distance between the poles or terminals and the dielectric constant of the material. When the voltage stress exceed what is called the corona inception voltage or breakdown voltage for the area, a discharge will occur. Voids have lower dielectric constant than equivalent distance in the insulation material and will cause the stress on that area to be greater and therefore the void will be more prone to becoming conducting. A partial discharge occurs when the voltage stress is enough to sustain a spark but not strong enough to create a complete arcing.

When a PD occurs, it can cause material in its vicinity to vaporize which will release an acoustic sound pressure wave emanating from the PD source, which will cause local stress and strain on the material in which it travels. This will be analysed further in section 2.3 and section 2.4. It has been suggested that the resulting acoustic signal has a dominant frequency range of 20kHz to 400kHz but both higher and lower frequencies exist [3] [10] [11]. There are other indicators of PD's other than acoustic pressure waves, such as electrical current pulses and chemical effects on the insulation material. Sensing systems for all three effects have been developed.

2.3 Ultrasound sensing systems

Since the PD's suggestively emits a sound pressure wave in the frequency region of ultrasound, knowledge from ultrasonic sensing in general could be borrowed. A PD source could then be modelled by an ultrasonic transducer and the first step was to create an optical sensor that could detect this kind of signal. Much of the knowledge in this area was gathered from different applications of ultrasound sensing, most importantly non destructive testing (NDT). This section and the next gives some background and theory about ultrasound sensing and also introduces some optical sensing techniques and their respective pros and cons.

Ultrasound sensing has become important in several different applications, particularly within structural health monitoring. Here, the interest for NDT is big, and ideas have been presented of letting NDT become an integral part of the building structure which would allow for continuous monitoring of the structure. Various methods for damage monitoring has been developed over the years and according to Betz et al. [7], the most promising of the few NDT techniques considered sufficiently technically mature for use in smart materials is acousto-ultrasonics. The idea with this is to use two probes on the surface that needs to be investigated, one which induces ultrasonic strain waves into the structure and another probe to pick them up. By examining the transmitted and/or reflected wave, a structural damage can be detected and even located.

Important to note is that the transmitting probe needs a good coupling material between its surface and the material in which the ultrasound is to be induced. A good coupler is a substance that matches the acoustic impedance of the surface that needs to be investigated, to prevent all of the ultrasound energy to be reflected on the surface instead of being transmitted into the material. The amount of sound energy being reflected while travelling to a different material is discussed more in depth in the coming section 2.4

The receiving probe can have several forms and most commonly is the use of another ultrasonic transducer tuned to the same frequency as the transmitter or even the same transducer capturing the reflected wave as it comes back. It can also be a fiber optical probe which possesses some interesting abilities.

2.3.1 Optical methods and fiber Bragg gratings

Optical sensing methods for ultrasound have been used for a quite some time and even experiments on PD sensing has even been made f.ex. by Blackburn et al. [2] which utilized a fiber optic coil as a sensor. An alternate and promising method of optical ultrasound sensing however, seems to be the use of fiber Bragg gratings. The reason to consider using optical fiber in the first place is because of the advantages with optical sensing, compared to conventional methods. This is mostly because of the inherent ability of fiber optics to withstand harsh environments with its immunity against electromagnetic interference which enables such a sensor to operate where electrical equipment would have a hard time functioning.

There are several different proposed systems and techniques described in published material that are utilizing fiber Bragg gratings as sensors. The coming subsections will describe different sensing systems that were considered for the project and reasons why they were discarded or chosen.

2.3.1.1 Narrowband tunable laser

As described in section 2.1, the reflected spectrum of a fiber Bragg grating has similar characteristics to that of a bandpass filter with the center frequency being dependant on

the temperature and the grating period. This system is used and described by Betz et al. [7]. The general theory behind it is that if a laser is tuned to a wavelength corresponding to somewhere within the grating reflection spectrum, a certain portion of the laser power will be reflected. If the FBG reflection spectrum would somehow change its wavelength interval, that would also alter the amount reflected by the laser as a consequence. The reflected laser power would therefore be modulated by the change of the Bragg wavelength λ_B of the grating. Generally for most gratings, there are areas on the slopes of the reflection spectrum that are steep and which could be considered linear. By tuning a laser to a point in this linear area, a linear modulation of the FBG center frequency would then be achieved. An illustration of this is shown in fig. 2.2 and is borrowed from the informative paper of Betz et al. [7].

By the FBG being subject to strain waves (such waves are analysed in depth in section 2.4), coming f.ex. from an ultrasonic sound pressure wave, it would change its center frequency according to what was written in section 2.1 and in particular the elasto optic properties of the fiber according to eq. (2.4). By measuring the reflected optical power of the laser with an optical receiver it is therefore possible to obtain a signal of the strain wave since it modulates the Bragg wavelength, which in turn modulates the laser signal. This system was eventually chosen as the basis for the created PD sensor in the project.

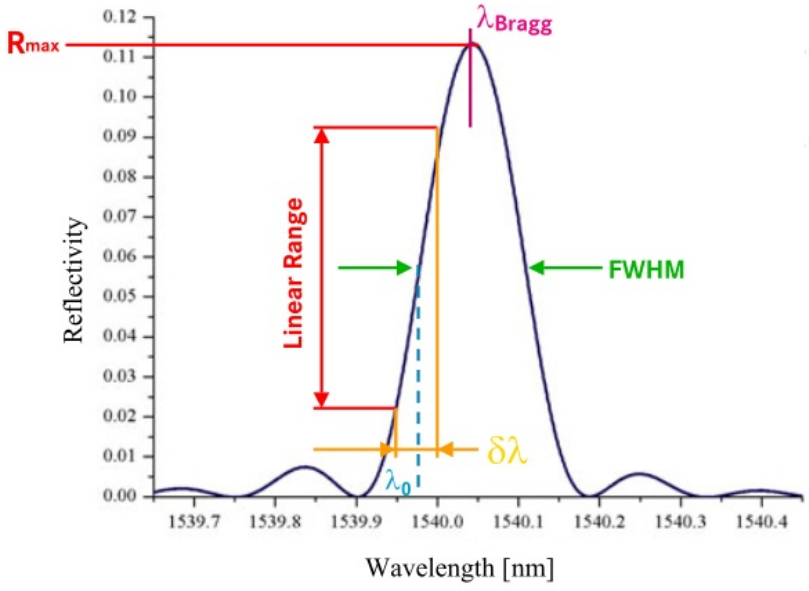

Figure 2.2: Theory for FBG sensing using narrowband laser

2.3.1.2 FBG overlap

Another interesting system involves using a broadband LED-source, instead of a narrow-band laser, and two tuned fiber Bragg gratings. The theory is to have the two grating spectra overlap on their slopes. By using two optical circulators, the light reflected from the FBG pair will be the overlap-area only. If only one of these gratings would be subject to a strain wave, that grating's center frequency will change while the other stays the same, which will consequently modulate the overlap area and therefore the reflected signal. This signal could be observed in a similar fashion as is described in section 2.3.1.1.

One advantage with this method is that it can be made insensitive to temperature change. If only one grating is exposed to strain but both are in the same temperature environment, the relative placement of the grating spectra with respect to the temperature will be constant while the strain modulation of the overlap still will be occurring. Problems with this method though is to tune the two gratings to overlap perfectly. Also, to be able to reap the benefit of the temperature invariance, one grating needs to be isolated from the strain waves while still being close enough to the sensing grating to share its temperature environment. These difficulties was ultimately the reason as to why this method was discarded in the project.

2.4 Sound waves in isotropic solid material

To be able to understand the readings, some knowledge of how waves travel through isotropic solid material is needed. The source used here has been the excellent book written by Heinrich Kuttruff [12]. A longitudinal wave is propagated in a solid material by the displacement of its particles around their equilibrium position. Such a wave consists of compressions and expansions of these particles. A compression means that a group of particles are closer to each other than when they are in their equilibrium state and an expansion means they are further away from each other. For an outgoing, longitudinal wave travelling in a thin bar the general expressions for the displacement, particle velocity, strain and stress are, by definition

$$u(x,t) = Af[a(t-\frac{x}{c_l})], \qquad \dot{u}\,(x,t) = \delta u/\delta t = Aaf'[a(t-\frac{x}{c_l})], \tag{2.5}$$

$$e_{xx}(x,t) = \delta u/\delta x = -\frac{Aa}{c_l}f'[a(t-\frac{x}{c_l})], \qquad X_x(x,t) = -\frac{AaE}{c_l}f'[a(t-\frac{x}{c_l})]$$

Strain is what is of interest since that is what the FBG function is related to. From eqs. (2.5) it follows that

$$e_{xx}(x,t) = -\frac{\dot{u}}{c_l}, \tag{2.6}$$

where c_l is the wave propagation speed for the given material and is defined as

$$c_l = \sqrt{\frac{E}{\rho}} \tag{2.7}$$

where E is the Young's modulus of the material and ρ is the material's density. The end of the rod can be described as a boundary between two materials (in the experiment this was perspex and air) and an incident wave here will give rise to a reflected wave that will travel back through the rod, and a transmitted wave that will go on and travel through air. This is simplified however because only longitudinal waves are considered, while in fact each reflection gives rise to a longitudinal and a transverse wave depending on the incident angle to the boundary. How much is reflected and transmitted is determined by the Fresnel formulas, relating the reflected wave B and the transmitted wave C to the incident wave A as follows

$$B = \frac{Z_1 - Z_2}{Z_1 + Z_2} A \qquad \text{and} \qquad C = \frac{2Z_1}{Z_1 + Z_2} A \tag{2.8}$$

The expression for displacement u for each part of the bar is therefore

$$u_1(x,t) = Af[a(t - \frac{x}{c_{1l}})] + \frac{Z_1 - Z_2}{Z_1 + Z_2} Af[a(t + \frac{x}{c_{1l}})] \tag{2.9}$$

At the boundary between the two materials, where $x = 0$, the following is true from eq. (2.9)

$$u_1(0,t) = (1 + \frac{Z_1 - Z_2}{Z_1 + Z_2}) Af(at) \tag{2.10}$$

and

$$u_2(0,t) = u_1(0,t) = \frac{2Z_1}{Z_1 + Z_2} Af[a(t - \frac{x}{c_{2l}})]$$

where u_2 is the transmitted wave into the material at the boundary. Eq. (2.10) says that the particles at the boundaries are displaced equally and that the reflected and incident waves wary synchronously. Since strain is given by $\delta u/\delta x$ the expression for strain at the boundary is given from the first part of eqs. (2.10) as

$$e_{xx}(0,t) = \frac{aA}{c_{1l}}(-1 + \frac{Z_1 - Z_2}{Z_1 + Z_2}) f'(at) \tag{2.11}$$

This means that depending on the acoustic impedances of the two materials a compressional wave for instance ($e_{xx} < 0$) may give rise to either a compressional or an extensional reflected wave. If $Z_1 < Z_2$, the reflected wave will be the same type as the incident wave. As an example, when the boundary is rigid ($Z_2 \to \infty$) a compressional wave will give rise to a reflected compressional wave. The other case where $Z_1 > Z_2$ the waves will be of opposite types. The best example here is when the boundary is free ($Z_2 = 0$), a compressional wave will create an extensional reflected wave. Eq. (2.11) also says that in the case of a free boundary the strain will be $e_{xx} = 0$. It also follows from the first part of eqs. (2.10) that the velocity at the boundary will be expressed as

$$\dot{u}\,(0,t) = aA(1 + \frac{Z_1 - Z_2}{Z_1 + Z_2})f'(at) \tag{2.12}$$

and in the case of a free boundary eq. (2.12) becomes

$$\dot{u}\,(0,t) = 2aAf'(at) \tag{2.13}$$

what this says is that when the boundary is free a compressional wave causes an extensional wave which doubles the particle velocity but cancels the deformation.

2.5 Laser Doppler vibrometer

A laser Doppler vibrometer (LDV) is an instrument commonly used to measure the velocity and displacement of a vibrating surface but has also been used to measure pressure fluctuations in an interfering substance. The basic function of the LDV is described in a paper by Joris Vanharzeele et al. [13]. To measure the vibration of an object, a laser beam is at first split into a reference beam and a test beam. The test beam is the only beam that goes outside of the device and is focused on the surface of interest. A vibration of this surface will shift the frequency of the reflected light, in accordance to the Doppler effect, by the following formula

$$\Delta f = \frac{2v(t)\cos(\alpha)}{\lambda}, \tag{2.14}$$

where λ is the light wavelength and $v(t)cos(\alpha)$ is the time-dependant particle velocity component of the vibrating surface along the axis of the laser. The reflected beam is compared to the reference beam by a photodetector responding to the beat frequency of the two beams, giving the difference in frequency, which holds a relationship with the velocity of the moving surface as in eq. (2.14). The output is often given as a voltage with a direct relationship to the particle velocity.

CHAPTER 3

Method

3.1 Fiber characteristics

To determine the FBG sensitivity, it was suggested that three variables needed to be investigated and determined. These three were all based on the properties of a FBG and its response to strain according to what is described in section 2.1. The variables are

$$\frac{d\lambda}{d\epsilon} \qquad \frac{dP}{d\epsilon} \qquad \frac{dP}{d\lambda}. \tag{3.1}$$

where $d\lambda/d\epsilon$ corresponds to the elasto-optic properties of eq. (2.4) which describes how much strain is needed to change the Bragg wavelength a certain amount. The other describes the change laser output power with respect to strain and Bragg wavelength shift respectively. They are there to give a direct value that can be used to get expected output voltage with a given input power, depending on the optical receiver available.

To properly measure these values, a controlled way to apply strain to the fiber while measuring the change in center frequency and output power was needed. The equipment used were, among other things, an optical spectrum analyser, a tunable laser in the 1550nm region, a broadband LED-source and an optical circulator, all set up as shown in fig. 3.1 with a few variations. Each procedure to determine each part of eq. (3.1) will be presented here in a separate section.

3.1.1 Change in wavelength with respect to strain

The first value investigated was the first part of eq. (3.1). As stated before, a controlled way of applying strain to the fiber was needed. Strain is defined as

$$\frac{\Delta L}{L} = \epsilon \tag{3.2}$$

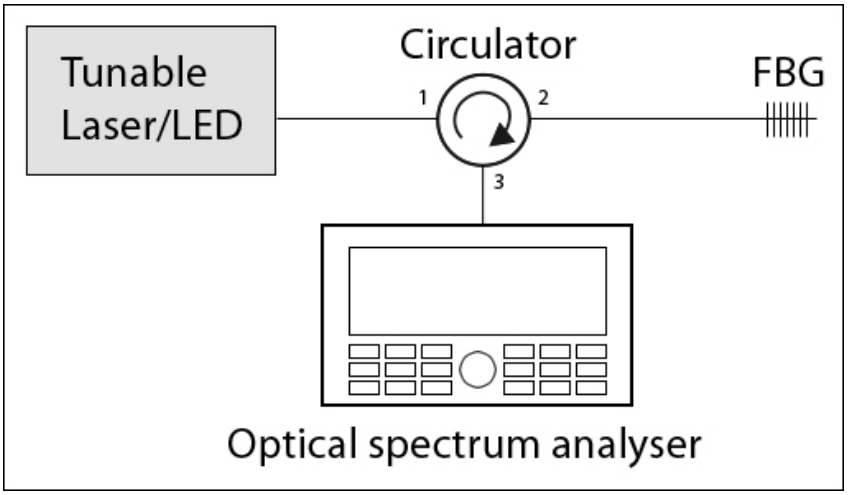

Figure 3.1: Setup for FBG sensitivity characterization

which led to the idea of creating a stretching mechanism where a fiber of length L could be precisely stretched by a distance ΔL to get strain acting on the fiber in the $\mu\epsilon$ regions. A mechanism as seen in fig. 3.2, was designed and constructed. The boxes on each side of the grid are sliders, each controlled by a micrometer. On top of each slider is a clamping piece that holds each end of the fiber in place. Both of the sliders' position could be adjusted and the distance between them represents L in eq. (3.2) while the micrometers controls the added ΔL and therefore the strain acting on the fiber. While adding strain in small increments, the center frequency of the reflected spectrum by the FBG from a broadband LED-source was monitored by an optical spectrum analyser and plotted, all with the equipment set up as in fig. 3.1. A minor note is that the increments with which the strain was added could in this case be made in bigger steps because of how wide the spectrum of the LED-source was, meaning the reflected spectrum would still be inside the transmitted LED-spectrum, and fully reflected, even if the center frequency of the FBG changed by quite a bit. This made potential small errors in the micrometer stretching distance ΔL less significant.

3.1.2 Change in output power with respect to strain

To determine the second value of eq. (3.1) a very similar procedure as the one just described was used. This experiment also utilized the constructed stretching mechanism seen in fig. 3.2 and had the same setup according to fig. 3.1. The difference here was that a tunable laser with a narrow bandwidth was used as source instead of a broadband LED. By tuning the laser to right above the of the FBG spectrum and stretching the fiber with the stretching mechanism, the FBG spectrum will move up in frequency and over the narrow laser, making more and more of it to be reflected. By applying small

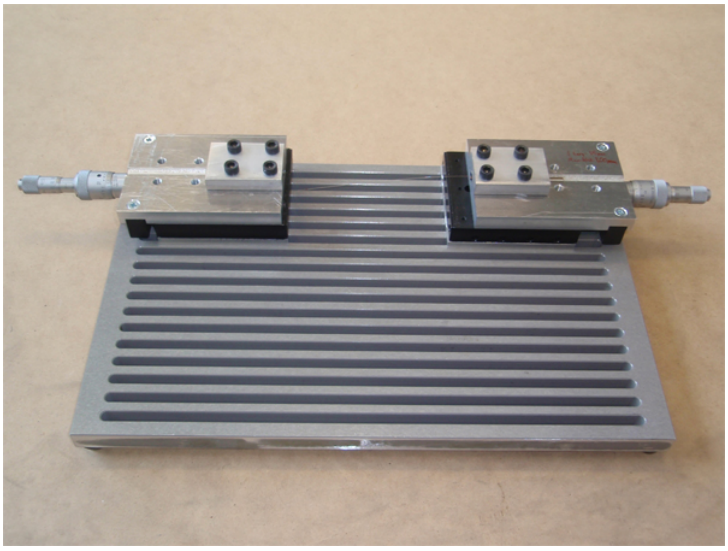

Figure 3.2: The constructed fiber straining mechanism

increments of strain while plotting the output power of the laser, as seen on a spectrum analyser, it was possible to get the value of interest from the slopes of the plot, which will be presented in chapter four. Since the shift in wavelength was sensitive to the strain applied, the increments in strain were made by very small steps which increases the influence of potential errors in the micrometer stretching distance ΔL.

3.1.3 Change in output power with respect to wavelength shift

The last sensitivity variable of eq. (3.1) could be calculated from the first two but to investigate if there was any coherency between the experiments, this was also measured experimentally. With the same setup as shown in fig. 3.1, with a tunable laser as source, the output power and the wavelength of the laser was observed on the optical spectrum analyser while simply tuning the laser wavelength with small increments over the entire spectrum of the FBG. There was no usage for the straining mechanism in this experiment other than putting some tension on the fiber to get the conditions as similar to the other experiments as possible.

3.2 Detection of ultrasound

After sensitivity had been estimated with the experiments presented in section 3.1, the next step was an attempt at making a working sensing system for detecting controlled ultrasonic pulses. To be able to induce the ultrasonic sound waves from the transducer into straining the fiber, it was determined that the FBG needed some kind of waveguide to which it was attached, that could pick up the sound waves more efficiently than the

thin area of fiber. Several methods of attaching the fiber to its waveguide were tried, including using adhesive tape following the example of a previous experiment conducted by Loock et al. [14] Because of the small amplitudes of the ultrasonic pulses, it was apparent that a stronger attachment to the waveguide was needed, and after consulting the written material by Trutzel et al. [15] it was decided that a strong two-component glue would be used.

The waveguide would need to consist of a well known material that would be able to carry the ultrasonic waves and also something that could be used in the high voltage lab when creating PDs. Based on this, and other papers who described using the same thing, perspex was chosen as the initial waveguide material. To maximize the chance of success, a perspex rod was used to match the circular shape of the ultrasonic transducer and a FBG was glued close to one end to be near the source. A gel used in medical ultrasonography was used as a coupler, the importance of which is described in section 2.3, and was applied between the transducer and the end of the perspex rod. A pulse generator fed the transducer with a short square pulse with a on time corresponding to double the frequency of the transducer. The off time was made sufficiently long so that each pulse from the transducer had time to ring by itself and die before the next pulse arrived.

The sensing system used was built on the one described in subsection 2.3.1.1 and the entire setup is illustrated in fig. 3.3. The optical receiver used, had a built in low-pass filter that could be set to either 35MHz or 125MHz depending on the desired transconductance value. The electrical filter that followed the receiver was a simple self-constructed high-pass filter that would remove an irregular low frequency component that made the signal hard to trigger on and read. It was constructed based on the 50Ω output resistance of the optical receiver to create a cut-off frequency around 10kHz by using a simple discrete RC filter with a capacitor with capacitance $100nF$ in series with a resistor with resistance $1k$ and having the voltage taken across the resistor.

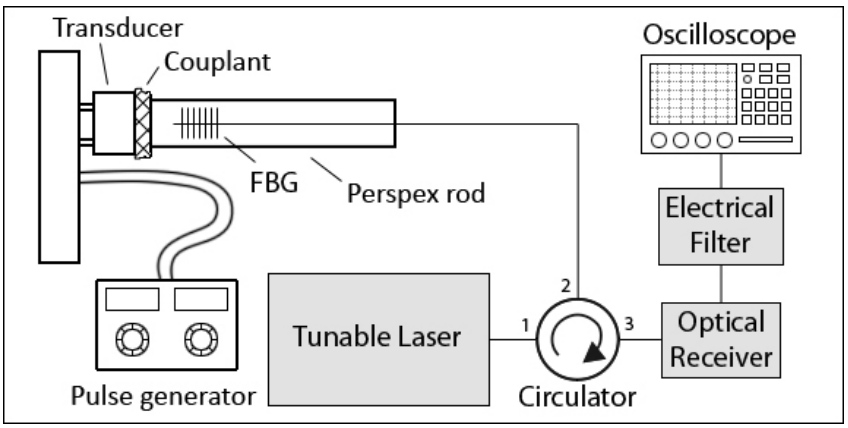

Figure 3.3: Experimental setup for ultrasound sensing

3.3 Experiment confirmation

Now that there was access to readings from an ultrasound sensor, an attempt to confirm the previous characterization of the fiber, determined with the stretching mechanism, was made with a calibrated measurement technique to determine the strain. This included the use of a laser Doppler vibrometer (LDV) to measure the particle velocity at the end of a perspex rod when exposed to ultrasonic pulses from the other end. A schematic of the experimental setup is shown in Fig. 3.4

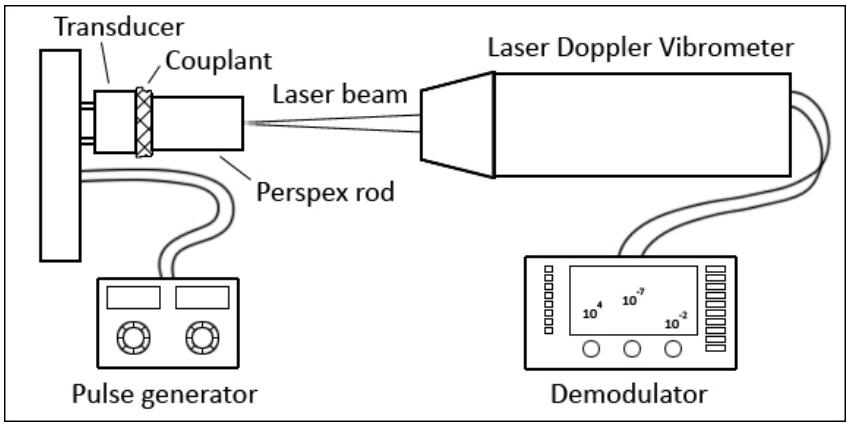

Figure 3.4: Experimental setup with laser Doppler vibrometer

In the experiment, a shorter perspex rod with a length corresponding to the position of the grating on the longer rod was placed on the transducer using the conductive gel as a coupler. The DV's laser was focused at the end of the rod while the transducer was fed with a step pulse, making it ring to its resonant frequency.

For the setup that was used, the boundary at the end of the rod consisted of perspex and air. This is roughly the case with a free boundary which means the observed particle velocity would then have to be divided by 2 to get the velocity, $\dot{u}$, of any particle not at the end of the rod according to eq. (2.13). With these readings, it is then possible to calculate the strain at any given point by using eq. (2.6) and multiplying that with the observed value of the second part of eq. (3.1), $dP/d\epsilon$, will produce a theoretical pk-pk output power from the FBG sensing system described in section 3.2. The expected voltage output can be obtained by adding to this, the formula eq. (3.3) found in the receiver manual for converting input power to output voltage. Combining everything gives the formula of eq. (3.4)

$$P \cdot Resp \cdot T_k \cdot G = V_{out} \tag{3.3}$$

$$\frac{\dot{u}}{2 \cdot c_l} \cdot \frac{dP}{de_{xx}} \cdot Resp \cdot T_k \cdot G = V_{out} \tag{3.4}$$

where $Resp$ is the responsivity, T_k the transimpedance and G the gain of the receiver. After calculating the value of eq. (3.4) with the gathered variable values, the result could be compared to the actual measured output values from the ultrasound experiment to see if they had a reasonable match which, if they did, would give credibility to the experimentally determined fiber characteristic value $dP/d\epsilon$ which was obtained by the method described in section 3.1.2.

3.4 Detection of partial discharge

The last step and final goal of the project was to create a working detector for partial discharges (PD's), building on the experience from the ultrasound sensor. A controlled way of creating the PD's in a lab environment was needed. The challenge with this part was to make sure that the theoretical acoustic pulse from the PD's were induced into the material where the fiber sensor was mounted. This section will describe the setup including the equipment used and the general method of how PD's were generated in the lab. Additionally, there will be two subsections describing the detailed individual setups used for the two different materials around which PD's where generated.

The first step in this experiment was to simulate a void appearing within an insulating material and to expose it to a high voltage stress field. As described in section 2.2 this will, if the voltage over the insulating material is high enough, create sparks in the void. The idea then was to mount the fiber sensor created earlier in the vicinity of the sparks with the desire to obtain readings of their acoustic signal. The first material used to create the artificial void and mount the FBG on, was perspex plates.

3.4.1 Perspex

An already used methods for creating sparks in high voltage labs is to sandwich plates of perspex between a brass cylinder and a plane. One of the perspex plates has a drilled hole in it which f.ex represents the void in an insulation. When high voltage is applied between the cylinder and the plane, sparks will be generated in the void. An illustration is given in fig. 3.5.

Using this method and mounting the FBG sensor in a similar fashion to what is described in section 3.2, an attempt was made to detect the PD's. The sensing system is basically the same setup as the ultrasound sensing system with the perspex rod except for where the fiber is mounted. As always, the laser was tuned by feeding the reflected signal to an optical spectrum analyser to visually determine the working point in the slope of around the Bragg wavelength of the FBG.

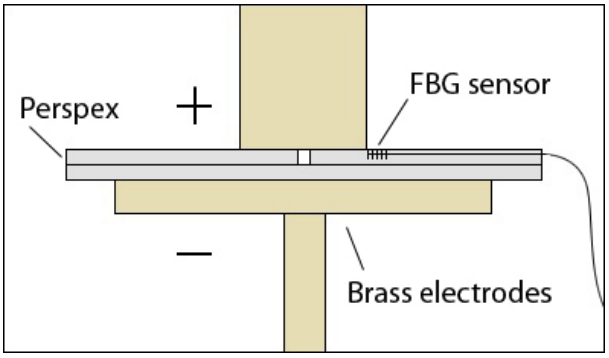

Figure 3.5: The placement of the fiber sensor in the hight voltage spark generator setup

3.4.2 Silicon rubber

Although perspex is an electrically insulating material, it is not very common in practice as a high voltage insulator. To try and connect this project with a practical situation, an experiment with a commonly used material was made. Silicone rubber is often used as an insulator in high voltage cables and wires.

In this project, a two component silicone rubber substance with a cure time of around twelve hours was used. Before the silicone cured it was a viscous substance which could be molded into a desired shape and form. A drawing of a shape was made that would fit into the high voltage spark arrangement, with a built in void where the sparks were wished to be generated, and a corresponding mold was constructed in the mechanical workshop.

A difference to the the perspex experiment of section 3.4.1 was the way that the FBG sensor was mounted. Instead of glueing, a new method was used that presumably had never been attempted before. When casting the silicone rubber in the custom made mold, the FBG was embedded into the sample in the process. An illustration of how it was set up in the high voltage lab when generating sparks is shown in fig. 3.6.

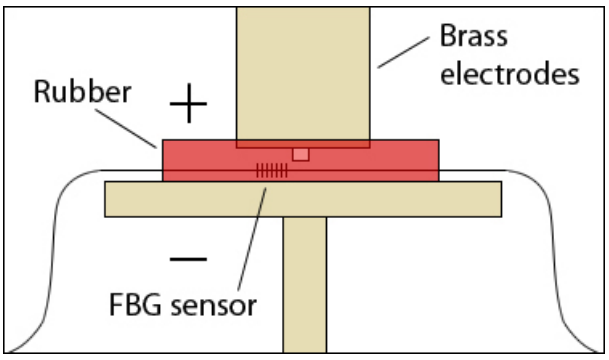

Figure 3.6: The placement of the fiber sensor in the hight voltage spark generator setup

CHAPTER 4

Results

4.1 Fiber characteristics

In this section the results from the experiments described in section 3.1 and will give a value for each of the variables in eq. (3.1). When performing the experiments, the values were recorded by hand and input into MATLAB where they were plotted.

4.1.1 $d\lambda/d\epsilon$

The first experiment involved stretching the fiber and observing the shift of the Bragg wavelength of the grating as described in section 3.1.1. The expected result was for the shift to be linear by looking at eq. (2.1). The plotted result is shown in fig. 4.1 and by using a linear fit function in MATLAB, the value of the constant could be determined as

$$\frac{d\lambda}{d\epsilon} = 0.7626pm/\mu\epsilon \tag{4.1}$$

which is a bit lower than the value of $1.2pm/\mu\epsilon$ which is what Phung et al. describes as typical [1]. The result however, was linear as expected. Reasons why the value differs from the ones of Phung et al. will be discussed in chapter 5.

4.1.2 $dP/d\epsilon$

The next value investigated was the change in output power while stretching the fiber, as described in section 3.1.2. Only one slope of the fiber was measured and the output values recorded by hand. Similar to the previously described procedure, the values were input into MATLAB and since a part of the slope was expected to be linear, a linear curve fit was applied to the plot shown in fig. 4.2 for the values between 20% and 80% of the difference between the output value at the maximum reflection and the noise floor.

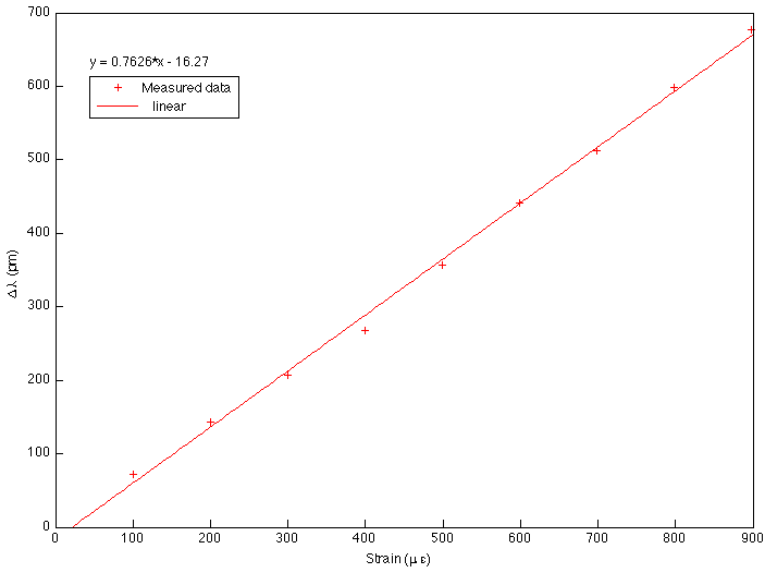

Figure 4.1: Plotted result of shift in wavelength with respect to strain.

The inclination constant of the slope gave the value

$$\frac{dP}{d\epsilon} = 2.226\mu W/\mu\epsilon. \tag{4.2}$$

The slope values were not as linearly aligned as might have been expected, which can be seen in the plot depicted in fig. 4.2. This will also be discussed in chapter 5.

4.1.3 $dP/d\lambda$

The final variable in the attempt to characterize the fiber was the change in output power with respect to shift in wavelength. The method for this experiment is described in section 3.1.3. The expected result here was to get an outline of the grating spectrum around its Bragg wavelength and, similar to when calculating $dP/d\epsilon$, to be able to apply a linear fit on both of its slopes. This was done in MATLAB and the slope ranges were made out of values between 20% and 80% of the difference between the maximum output value and the noise floor. The values for the two slopes differed but for comparability with the other experiments, the left slope value is presented here as

$$\frac{dP}{d\lambda} = 2.926W/pm. \tag{4.3}$$

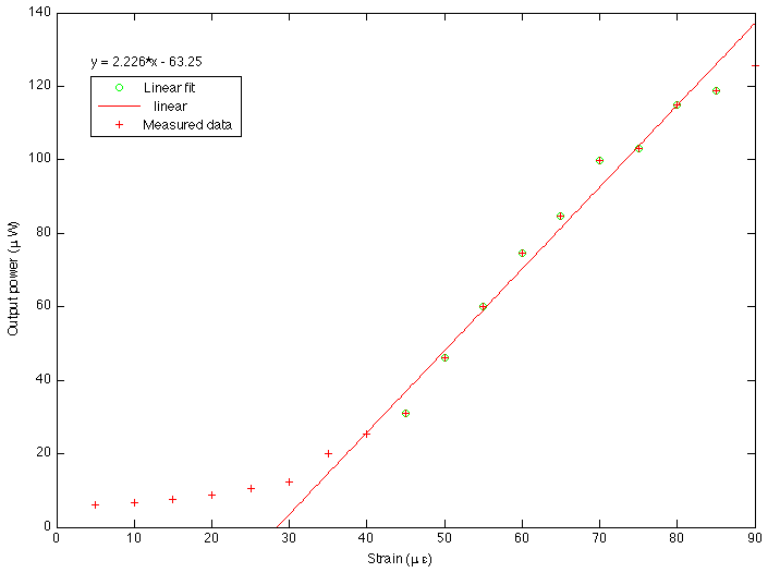

Figure 4.2: Plotted result of change in output power with respect to strain.

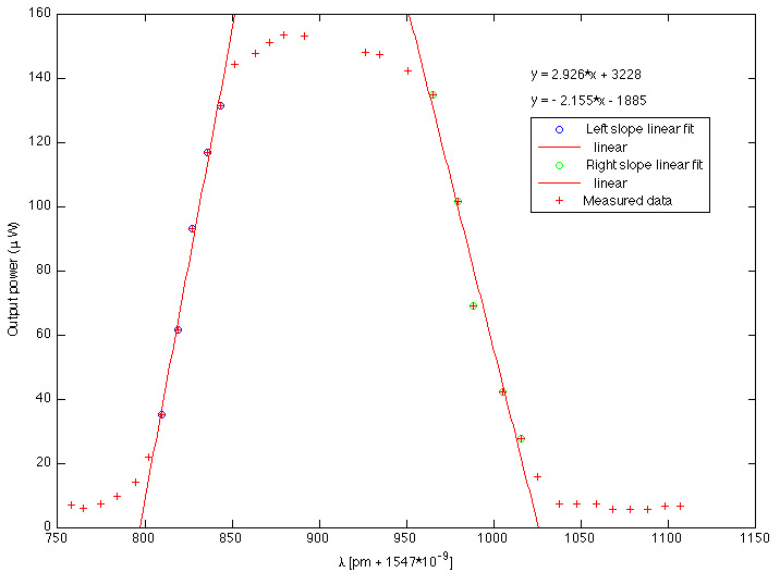

Figure 4.3: Plotted result of shift output power with respect to shift in wavelength.

To get an indication whether or not these values were had any coherency the following observation was used

$$\frac{d\lambda}{d\epsilon} \cdot \frac{dP}{d\lambda} = \frac{dP}{d\epsilon} \tag{4.4}$$

and inputting the values from all the experiments yielded the following result

$$0.7626 \cdot 2.926 = 2.231 \mu W/\mu\epsilon \tag{4.5}$$

which correlates well with the experimented value. However, the different values for the slopes forced caution when performing the ultrasound test and both slopes of the spectrum were used for modulating the laser in those tests, to investigate whether or not it mattered which side of the spectrum the laser was pointed at.

4.2 Detection of ultrasound

This section will present the result from the measurements with the ultrasound sensor described in section 3.2 and will also give the results from the laser doppler vibrometer experiment described in section 3.3.

With the sensor mounted on the perspex rod and the rod attached to the transducer with the coupling gel, the transducer was fed with a step pulse of double the frequency it was specified to emit. Reasons for this is also described in section 3.2. This made the transducer ring to its resonance frequency, which in this case was around $200MHz$, and the reading from the fiber sensor can be seen in fig. 4.4 with a pk-pk value of approximately $26.8mV$.

To confirm the previous sensitivity characterization values presented in section 4.1, a calibrated measurement of the particle velocity was made with a laser doppler vibrometer (LDV), with the methods described in section 3.3. The readings from the LDV can be seen in fig. 4.5 and are saying that the maximum pk-pk particle velocity was in the area of $7 \times 10^{-3} m/s$, since the DV scale was $10^{-2} \frac{m}{s}/V$ and the voltage levels observed were about $700mV$ maximum.

With numerical values inserted into (3.4), using $dP/de_{xx} = 2.226W/e_{xx}$ as determined in section 4.1 and $c_l = 2860m/s$ as the wave propagation speed in perspex given by the book written by Kuttruff [12].

$$\frac{7 \times 10^{-3}}{2 \times 2860} \cdot 2.226 \cdot 0.8 \cdot 14000 \cdot 1 \approx 30mV. \tag{4.6}$$

The calculations corresponds well with the observed voltages presented above for the sensor readings in the ultrasound experiment. This confirms the experimentally determined value of eq. (3.1.2).

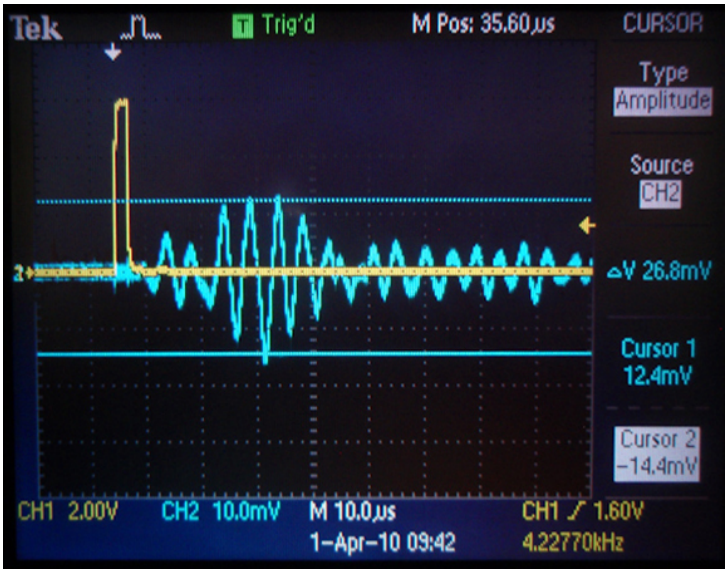

Figure 4.4: Signal from the FBG

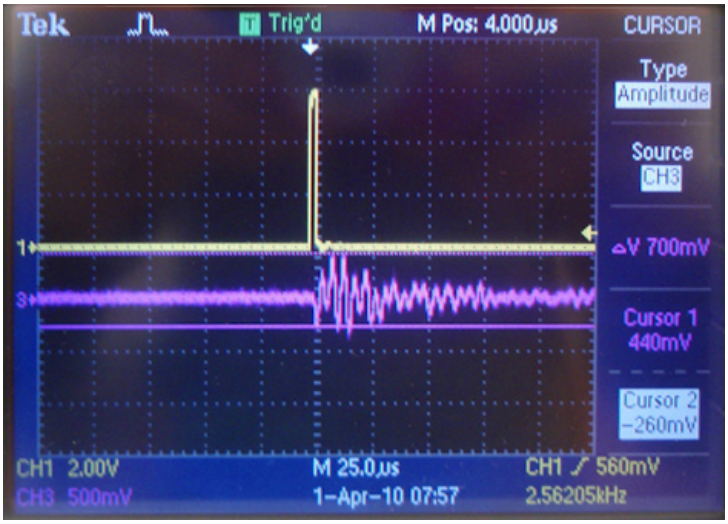

Figure 4.5: Particle velocity measurement

4.3 Detection of partial discharge

The last and most important experiment was the attempt to get readings from partial discharges in the high voltage laboratory. This experiment was divided into two parts, one attempt with the fiber mounted on a perspex surface and one with the fiber embedded into silicone rubber. Before presenting the results for each of these tests, some general results and measurements will be given.

When PD's were generated in the lab, they were picked up electronically through

a conventional method of PD detection and showed up on the oscilloscope as short voltage spikes which were used for triggering. Electronically these spikes had a very high frequency in the MHz range but for the acoustic signals, lower frequencies were expected.

What should also be noted is that there were electromagnetic interference present even though the entire motivation for the project built on eliminating them. The reason being that electronic circuits were used to filter and output the signals to the oscilloscope and they were located in the unshielded lab in close vicinity to the high voltage source. The interference picked up can be seen in fig. 4.6. Fortunately, since the interference is shorter and has higher frequency than the acoustic signals, they did not affect the final result.

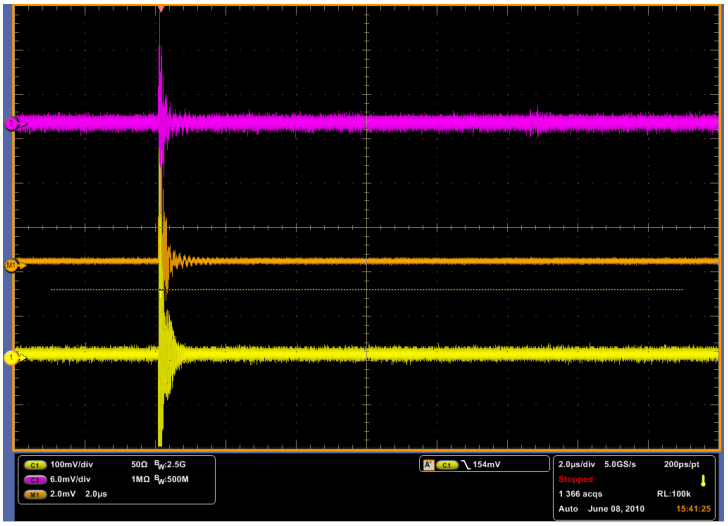

Figure 4.6: Electromagnetic interference picked up in the test area.

In the plot, the topmost waveform represents the real-time signal from the FBG, the middle being an average of the former and at the bottom is the electrical signal from the conventional PD detector. This will be the case for all the coming figures.

Mentioned in section 3.2 was an irregular low frequency component to the signal that was filtered through a simple high-pass circuit (which is also the circuit that helped pick up the electromagnetic interference mentioned above). Without any specific values, an example of the shape of this disturbance is shown in fig. 4.7. This noise was never fully investigated but theories about unwanted reflections in the optical systems causing constructive and destructive interference which could explain the noise's behaviour of seemingly jumping between two extreme levels at random. All this unwanted noise made all the readings difficult to see even after filtering. Investigating and eliminating this disturbance source is something that would be of high priority for future work when

building on this project.

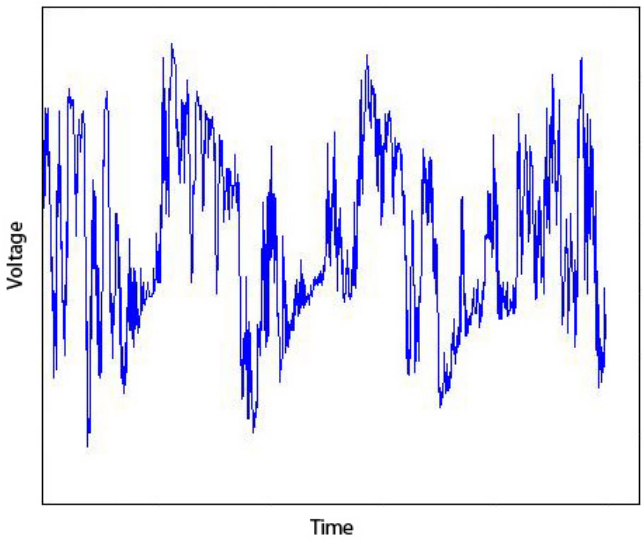

Figure 4.7: Low frequency noise present during the experiments.

4.3.1 Perspex

For the perspex attempt, the setup described and visualised in section 3.4.1 was used. Sparks were generated at a voltage level around $10kV$ and the sensor was mounted as close to the source as possible with consideration for the inherit directivity of the sensor discussed in section 2.1, again referring to fig. 3.5 for visualisation. For testing purposes, this mounting of the fiber was exposed to ultrasound from the transducer used in the formal ultrasound experiment and, even though no formal testing and documentation of this characteristic was made, a clear directivity could be seen for the sensor when placing the transducer at different angles to the fiber axis on the perspex plate.

When creating PD's, the results were not very clear by inspection, as seen in fig. 4.8 which is a zoomed in screen shot of the oscilloscope that tried to focus on one single PD, but by inputting the data into MATLAB and performing a Fast Fourier Transform (FFT), the result becomes clearer. In fig. 4.9 the frequency spectrum is shown of the optical output when no sparks were generated and in fig. 4.10 the same spectrum is shown but with partial discharges being generated. The time segment that the FFT is based on was sufficiently long to contain several discharges.

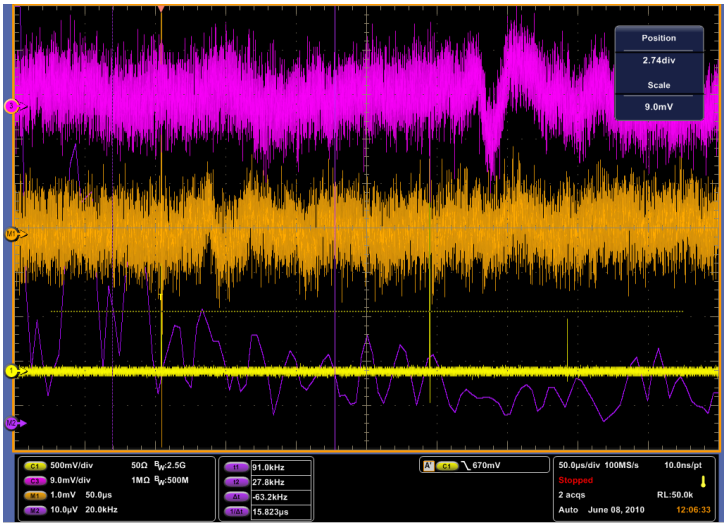

Figure 4.8: Waveforms from the oscilloscope when PD's were generated on the perspex sample.

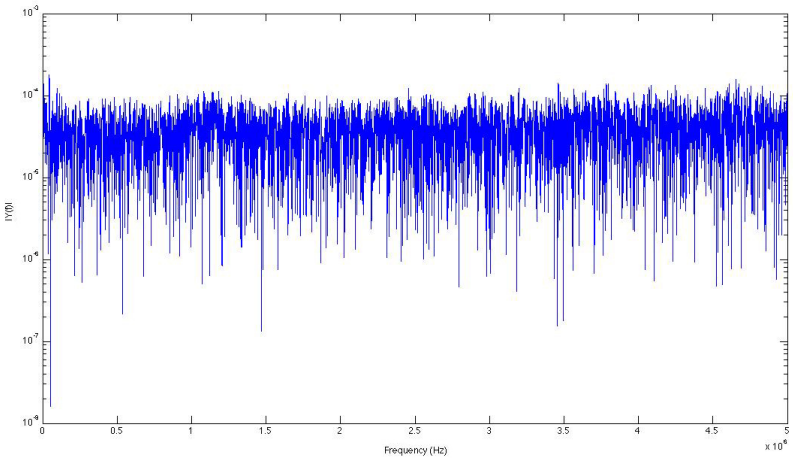

Figure 4.9: Frequency spectrum of the sensing system connected with the perspex sample without any sparks being generated.

Figure 4.10 shows that some content had been added higher up in frequency than expected when the sparks were generated. This image must be compared to the spectrum for the electrical signal that represents the sparks, as shown in fig. 4.11 to try and eliminate the idea of the added content being the RF noise seen in fig. 4.6.

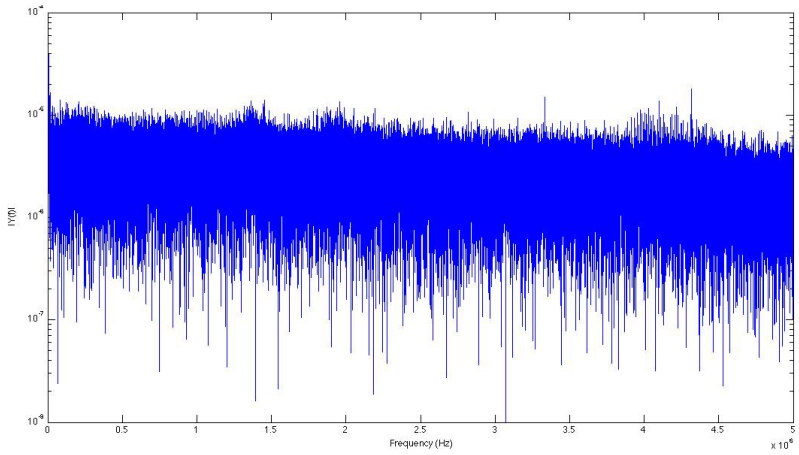

Figure 4.10: Frequency spectrum of the sensing system connected with the perspex sample with sparks being generated.

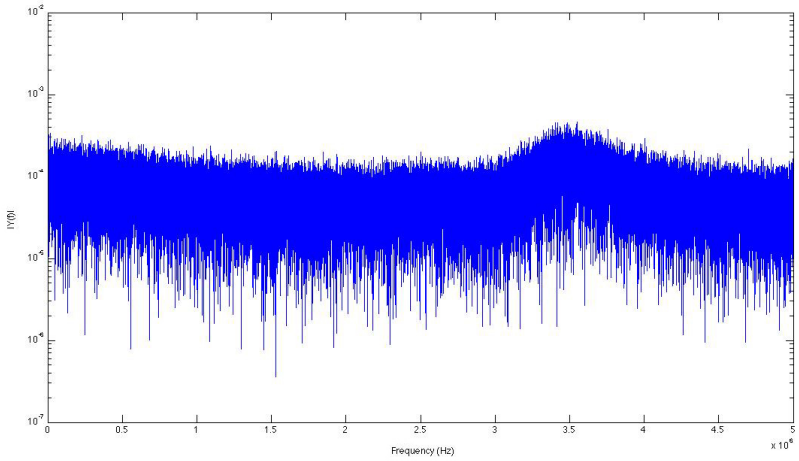

Figure 4.11: Frequency spectrum of the signal from the electrical PD sensor.

4.3.2 Silicone Rubber

The same setup that was used for the perspex sample described in the previous section was also used for the silicone rubber sample. This time the fiber was embedded in the sample as explained in section 3.4.2. This construction allowed the sensor to come closer to the source and it is likely that the connection with the FBG and the rubber, which was supposed to act as the waveguide, was better than when using glue to mount the fiber. An overview image of the waveforms can be seen in fig. 4.12 with the middle one being an average of the topmost signal from the optical system. The result here was

much clearer by inspection but the question remains if it was the sparks that generated the output or if it was something else. The FFT of the non-averaged signal is shown in fig. 4.13 which is zoomed in on the lower frequency spectrum since the higher frequency spectrum contained no peaks above the noise floor.

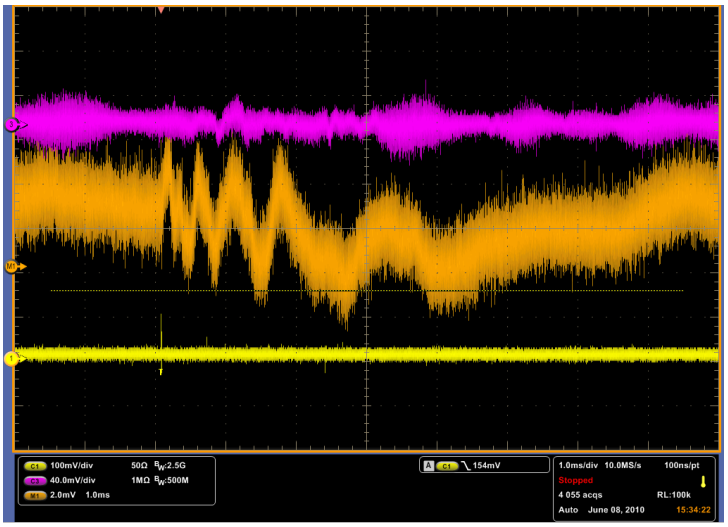

Figure 4.12: Waveforms from the oscilloscope when connected to the rubber sample with sparks being generated.

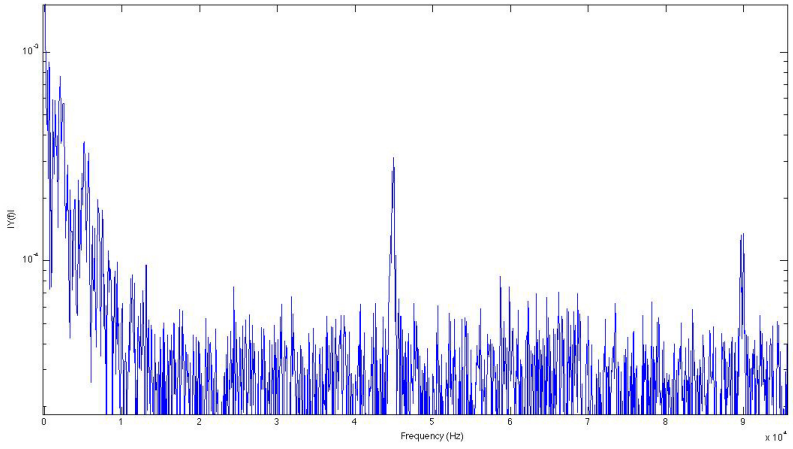

Figure 4.13: Zoomed in frequency spectrum of the optical signal with the system connected to the rubber sample while sparks were generated.

CHAPTER 5

Conclusion

5.1 Thesis conclusion and result discussion

The main question that this thesis was meant to answer was stated in section 1.2. It was asked whether or not an FBG could be used as a sensor for the acoustic impulse from partial discharges in high voltage equipment. This section will try to answer that question based on all the information given throughout the report.

5.1.1 Ultrasound sensor

In papers published earlier by others, the FBG has already been proven to be viable as a sensor for ultrasound. That was again confirmed in this project with the results in section 4.2, displaying a sensor placed on a perspex rod successfully detecting the ultrasonic pulses emitted from a transducer. The experiment was followed by a sensitivity calculation to estimate the probability of PD detection. Since the results of eq. (4.2) together with the receiver formula eq. (3.3) showed that the required strain to get a noticeable reading was in the $\mu\epsilon$ range, which is also the strain levels related to lamb waves in the ultrasonic frequency region according to Betz et al [7]. This was satisfying to a sufficient enough degree for the project to move on to building a test-prototype for PD detection in the high voltage laboratory.

5.1.2 PD sensor

The results from the PD detection is not as easily interpreted as the ultrasound results. There are several factors to consider and in this section, every result plot will be analysed and discussed.

First off are the perspex sample plots. As can be seen from the waveforms depicted in fig. 4.8 there was not really a signal clear enough to draw any conclusions from. By bringing the data into MATLAB and performing an FFT to plot the frequency content,

some interesting observations could be made. By comparing the three images fig. 4.9, fig. 4.10 and fig. 4.11 some careful conclusions could be drawn that some additional content had been added to the frequency spectrum of the optical sensor output signal, and that this could possibly be the FBG reacting to the partial discharges. This is because there are no peaks in the case where no sparks were generated, and the peaks that appeared when they were generated were not of the same frequency as the electronically detected sparks.

For the rubber sample there were clearer visual results but the source of the readings could not be determined with certainty. Peaks in fig. 4.13 showed some signal in the area of $45kHz$ and around $90kHz$. This indicates a distorted signal with $90kHz$ possibly being a harmonics to the peak at $45kHz$. Unfortunately there are tendencies for a peak at $45kHz$ in plots when no sparks were generated even though it was stronger when they were, and even though the $90kHz$ peak only could be seen when the sparks were occurring, it cannot be said with certainty that these peaks are the acoustic signal from the sparks sensed by the FBG.

These results are somewhat disappointing since it could not be stated with a hundred percent certainty that the partial discharges were successfully detected by the FBG. However, the results still proved that the sensor was capable of sensing if the strain was present through the ultrasound experiment. It was also indicated through the high voltage experiments that something was sensed but due to noise and interference in the system, the signals could not be completely defined.

To answer the question stated in the beginning of this section and this report - whether or not an FBG could be used as a sensor for the acoustic impulses for partial discharges in high voltage equipment - the answer is probably. The results show promising potential but more needs to be known about the acoustic characteristics of a PD and more testing needs to be done in the high voltage laboratory.

5.2 Thesis contribution

Earlier publications have treated the use of fiber Bragg gratings as ultrasound sensors with several different applications. However, the application in the area of high voltage and as a partial discharge sensor has not been widely researched. When this project was undertaken, only one paper could be found that wrote about the usage of a fiber Bragg grating in this particular area [1], but that was only in theory. No previous paper that could be found had conducted practical experiments with generated partial discharges. That was done here in addition to a new innovative method of embedding the FBG into high voltage insulation material, in this case silicone rubber. This thesis will act as a first step and a building stone for future research, possibly in the form of a Ph.D.

5.3 Future work

There is much more that needs to be done in this area until a proof of theory has been established and even more until a working prototype, that could possibly be used in a practical environment, could be created. Based on the results presented in this thesis, some recommendations for future work can be done. The optical sensing system needs to be fully investigated to be able to eliminate all the noise coming from unwanted reflections and other unknown sources. More testing needs to be conducted in the high voltage laboratory, with alternative environments where partial discharges are generated and with different mounting techniques, possibly building on the rubber embedding which in my opinion holds great potential. It would also be interesting to see if the stability of the optical sensing system could be improved by using a FBG with wider spectrum and less reflectivity. This might eliminate some noise caused by the laser moving but could also decrease sensitivity. A strong recommendation would also be to use fiber Bragg gratings that are shorter, regardless of the chosen maximum reflectivity. This based on what the previously written material has stated, as described in section 2.1. The ones used in this experiment had a grating length of $15mm$ and a reflectivity of 95

References

[1] B.T. Phung et al. Development of new partial discharge sensors for condition monitoring of power system equipment. *Australasian Universities Power Engineering Conference*, 2, 2005.

[2] R.E. James T.R. Blackburn, B.T. Phung. Optical fibre sensor for partial discharge detection and location in high-voltage power transformer. *Dielectric Materials, Measurements and Applications*, pages 33–36, 1992.

[3] T. Liang and W. Weilin. Method and apparatus for locating partial discharge in electrical transformers. *6th Int. Symp. on H.V. Engineering*, 1989.

[4] Gerald Meltz Kenneth O. Hill. Fiber bragg grating technology fundamentals and overview. *Journal of Lightwave Technology*, 15(8), August 1997.

[5] Matin Guy. Recent advances in fiber bragg grating technology. *La Physique au Canada*, 60(1), 2004.

[6] Ning Chenxiao and Zhang Xushe. Fiber bragg grating vibrating sensors and its signal processing system. *IEEE*, 2007.

[7] Daniel C Betz et al. Acousto-ultrasonic sensing using fiber bragg gratings. *Institute of Physics Publishing*, 10 January 2003.

[8] Graham Thursby et al. Structural damage location with fiber bragg grating rosettes and lamb waves. *SAGE Publications*, 6(4), 2007.

[9] Aldo Minardo et al. Response of fiber bragg gratings to longitudinal ultrasonic waves. *IEEE Transaction on Ultrasonics, Ferroelectrics and Frequency control*, 52(2), February 2005.

[10] Muhr Hans Michael and Schwartz Robert. Partial discharge impulse characteristics of different detection systems. Technical report, Institute of High Voltage Engineering and System Management Graz University of Technology, Austria.

[11] N.K. Roy S. Karmakar and P. Kumbhakar. Detection of partial discharges using optoelectronic method. *International Conference on Optics and Photonics*, 2009.

[12] Heinrich Kuttruff. *Acoustics: An Introduction.* Taylor & Francis, 2007.

[13] Joris Vanharzeele et al. Flow characterization using a laser doppler vibrometer. *Optics and Lasers in Engineering*, 45:19–26, 2007.

[14] Loock et al. Recording the sound of musical instruments with fbgs: the photonic pickup. *Applied Optics*, 48(14), May 2009.

[15] Michael N. Trutzel et al. Smart sensing of aviation structures with fiber-optic bragg grating sensors. *Proceedings of SPIE*, 3986, 2000.